Available online at www.sciencedirect.com

ScienceDirect

Energy Procedia 84 (2015) 221 – 227

Energy Procedia

E-MRS Spring Meeting 2015 Symposium C - Advanced inorganic materials and structures for photovoltaics

Optical performance of Ag-based back reflectors with different spacers in thin film Si solar cells

L.V. Mercaldo*, I. Usatii, E. Bobeico, F. Russo, L. Lancellotti, P. Delli Veneri

ENEA - Portici Research Center, P.le E. Fermi 1, 80055 Portici (Napoli), Italy

Abstract

We have compared different Ag-based back reflectors (BRs) applied to superstrate-type microcrystalline Si devices grown on Asahi U glass. In particular, substitution of the conventional ZnO:Al layer by MgF_2, with lower refractive index and no free-carrier absorption, has been investigated. As electrical issues can mask the optical performance of the BR when evaluated by EQE measurements, a purely optical method that compares the intensity of Raman spectra generated with long wavelength excitation light has been applied. Based on this investigation, MgF_2/Ag is potentially superior to ZnO:Al/Ag, even when MgF_2 is used in the form of ultrathin layer (few nm, likely island-like). Nevertheless, the novel dual-function n-SiO_x/Ag BR outperforms all the other BRs.

Peer-review under responsibility of The European Materials Research Society (E-MRS)

Keywords: Thin-film solar cells; μc-Si:H; Back reflector; Raman scattering

1. Introduction

Thin film Si solar cells make use of active layers with limited thickness due to poor transport properties and degradation issues. Proper light-management schemes are then needed to enhance the photo-current and ultimately the device efficiency. Textured substrates in combination with a back reflector are then employed to trap light in the absorber layer and different interface morphologies, both random and periodic, are being explored [1-7]. In

* Corresponding author. Tel.: +39-081-7723217.
E-mail address: lucia.mercaldo@enea.it

Peer-review under responsibility of The European Materials Research Society (E-MRS)
doi:10.1016/j.egypro.2015.12.317

particular, the back reflector has to provide for high reflectivity over a broad wavelength band and efficient scattering at large angles of the unabsorbed light, to maximize the optical paths back in the thin active layer [8]. One solution is the use of a metal back reflecting contact, typically Ag with excellent conductivity and good reflectivity. A thin buffer layer with low refractive index, like doped ZnO, is also inserted between Si and Ag, to avoid losses in reflected light due to surface plasmon absorption [9]. Back reflectors based on diffusive dielectric materials, such as white paint coatings or white sheets, are also in use [10]. Here we focus on the Ag-based design. The application of an alternative non-conductive dielectric buffer with refractive index lower than ZnO has been explored, for the potential benefit from both the lower *n* and the absence of free-carrier absorption. In particular evaporated MgF_2 with $n \sim 1.38$ at IR wavelengths has been selected, as also proposed in [11] and in [12] for thin film Si and Si heterojunction solar cells respectively. Different designs have been tested for the realization of proper local contacts. The optical performance has been evaluated in terms of reflectance and external quantum efficiency (EQE) with respect to the conventional BR configuration (ZnO:Al/Ag) and to the advanced dual-function n-SiO_x/Ag design [13,14]. Since electrical issues can affect the EQEs, we have also applied a purely optical method that compares the intensities of Raman spectra excited at a relevant wavelength (785 nm) as proposed in ref. [15], in order to gain insight on the full optical capabilities of the different BRs.

2. Experimental

The performance of the different Ag-based BRs has been evaluated when applied on 1 μm thick p-i-n μc-Si:H solar cells (superstrate configuration). The devices were grown on Asahi U glass with randomly textured SnO_2:F acting as transparent conducting electrode (TCO), including n-type μc-Si:H (n-Si) or n-SiO_x, 30 nm thick, as n-layer. Details on cell fabrication parameters are reported elsewhere [13,16,17]. The devices were completed with sputtered Al doped ZnO (80 nm thick) followed by evaporated Ag, with Ag only or with evaporated MgF_2 plus Ag. The devices with n-Si and completed with the commonly used ZnO/Ag BR were used as baseline. For each design, 1 x 1 cm^2 cells were defined by using a metal mask at the back contact fabrication step. A thermal treatment was applied to the finished devices to improve the metal contact (2h at 150°C in air). In addition, samples simulating the backside of the solar cell [TCO/μc-Si:H(200nm)/n-Si(30nm)/BR] have been fabricated for a purely optical preliminary investigation of the potential of the MgF_2/Ag combination.

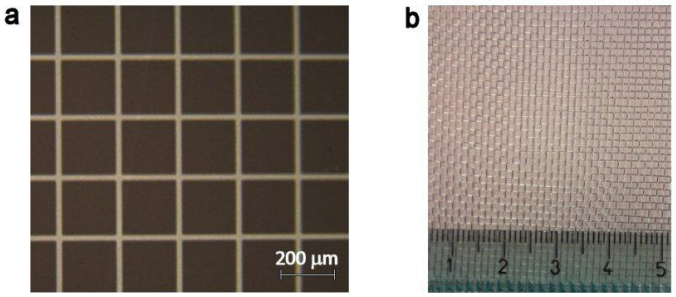

Fig. 1. (a) Plan view by optical microscope of MgF_2 patches (dark squares) realized by photolithography on the backside of a μc-Si:H solar cell; (b) Stainless-steel mesh used during MgF_2 evaporation in the shadow mask approach.

With the highly resistive MgF_2 buffer layer, manufacturing issues have been firstly tackled, as proper local contacts are needed in order to achieve good electrical performance. Both photolithographic techniques and use of fine metal meshes acting as shadow mask have been tried (fig. 1). Photolithographic lift-off type masks have been realized such that 80-85% of the cell back-surface would be covered with square MgF_2 patches with side varying from 200 to 400 μm and contact openings from 25 to 35 μm wide. Stainless-steel meshes available in the lab were used for a preliminary test in the shadow mask approach. The mesh had 1.06 mm aperture side and 220 μm wire size

that provides a MgF_2 coverage of only ~69% and a likely too large pitch between contacts with impact on the series resistance (R_s) of the solar cells. Also the application of ultrathin island-like MgF_2 layers has been tested, as recently proposed by Tokyo Tech [11], where the local electrical contact is achieved through the native openings in the non-continuous film. In this case a low growth rate has been selected (0.3 Å/s versus 2 Å/s for thicker layers).

The characterization included reflectance measurements with a PerkinElmer λ-900 spectrophotometer equipped with an integrating sphere, EQEs with Bentham PVE300 setup, current density-voltage characteristics under dual lamp WACOM solar simulator. In addition, Raman spectra were collected on the solar cells with a Renishaw inVia Reflex Raman spectrometer equipped with motorized xyz sample stage. The measurements were carried out in backscattering configuration with a long working-distance objective by using a 785 nm diode laser and focusing the beam through the substrate (glass + TCO) on the Si stack. In particular, the intensities of the Si optical phonon band at 520 cm^{-1} for different samples were compared. In order to obtain reliable absolute intensities, spectrometer settings and laser intensity were kept constant and z scans were acquired to avoid the inaccuracy in the optical focus definition. The microscope stage was scanned in the vertical direction so that the surface passed through the plane of focus of the laser beam. The spectra were recorded as a function of z position and a maximum was obtained for a certain z value (easily evaluated by plotting the integrated intensity in the 430 - 540 cm^{-1} range vs. z, as shown in fig. 2). As the sample is moved away from the focal plane, a larger area is being excited by the laser beam, so that the signal is a convolution of losses due to the surface not being in focus, and gains due to a larger volume being illuminated. The maximum is however expected for all the samples in the same focus condition in the present experiment with no variation of front TCO morphology in the solar cells. The spectrum with maximum intensity within the z scan set has been finally extracted for each sample.

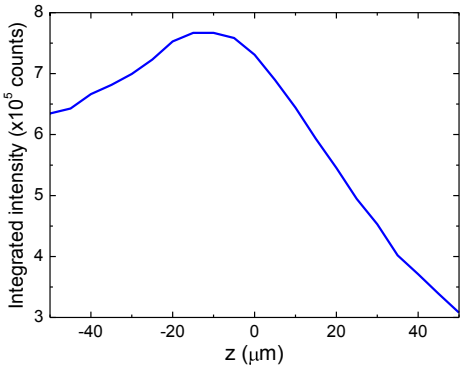

Fig. 2. Example of Raman depth profile on a μc-Si:H solar cell at excitation wavelength of 785 nm. The integrated intensity of the Raman signal in the range 430 - 540 cm^{-1} is plotted versus the vertical position (the position of visual focus was set as z=0).

3. Results

The potential of MgF_2 as buffer layer in Ag-based BRs has been firstly evaluated by studying the reflectance of samples simulating the backside of the cell, i.e. stacks with reduced μc-Si:H thickness with respect to real solar cells followed by the n-type layer and the BR, grown on the same TCO-covered glass as the solar cells to maintain the same rough interface morphologies. Fig. 3 shows the reflectance of such [TCO/μc-Si:H(200nm)/n Si(30nm)/BR] samples with different BRs as explained in the legend. For the MgF_2 buffer layer, the same thickness as the ZnO:Al layer has been considered or only few nanometers. With a thin μc-Si:H absorber, rather large reflectance is expected at long wavelengths as this portion of light is poorly absorbed. The very low reflectance obtained with the Ag BR (dashed line) is indication of the strong plasmonic absorption losses at the textured Si/Ag interface [9]. The insertion of the 80 nm thick ZnO:Al buffer layer significantly reduces these losses. Even larger reflectance is achieved with MgF_2(80nm)/Ag BR and interestingly with ultrathin MgF_2 layers (4-8 nm) the reflectance is already similar to the values measured with conventional ZnO:Al(80nm)/Ag BR.

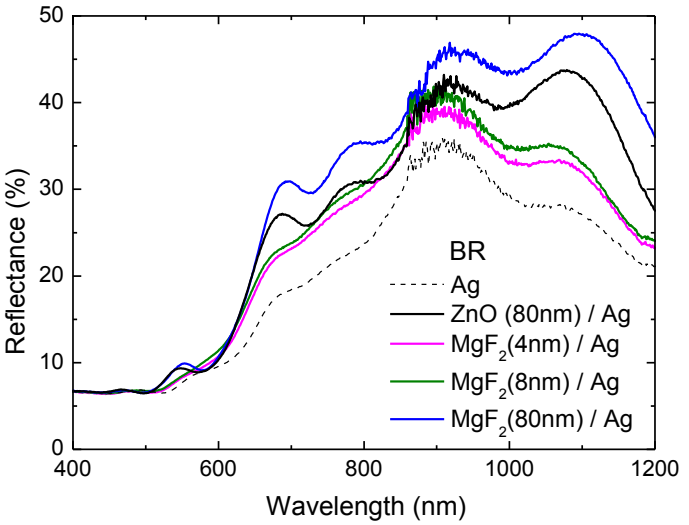

Fig. 3. Reflectance of TCO/µc-Si:H(200nm)/n-Si(30nm)/BR samples, simulating the backside of the solar cells, with different BRs.

The reflectance measurements in fig. 3 demonstrate the good potential of MgF_2 as very efficient buffer layer between Si and Ag. As for the actual cells however, both strategies for the application of relatively thick MgF_2 layers showed flaws. In the photolithographic approach, the witness cells (standard devices with no MgF_2 layer but going through all the process steps) revealed deteriorated performance. Adjustment of the process is then needed. With use of metal mesh, the cells showed inferior performance than the baseline devices due to both the non-optimal mesh geometry and shadowing effects (non-trivial perfect contact of mesh and sample is needed). With both the approaches the main impact was on the series resistance that showed additional deterioration after the final thermal treatment routinely applied to improve the metal contact. Also reduced J_{sc} relative to the corresponding baseline cell was measured, likely due to poorer charge collection, while the V_{oc}s were around 500 mV for all the devices. Also for the ultrathin approach, the present cells suffered from very large R_s and degraded charge collection, even when reducing the MgF_2 thickness to nominal 2 nm (based on the growth rate). After annealing, in this configuration the current flow was fully blocked in most cases. We suppose that the actual layers might be thicker than the designed values or coalescence of the islands in the discontinuous film may happen at a rather early stage with the selected growth technique, so that the layers do not present enough openings. In addition, the thermal treatment might have the effect of closing the gaps. Thickness control and formation of proper island-like patterns is very critical and might favour the use of sputtering, as in the Tokyo Tech approach [11], instead of thermal evaporation, as available in this investigation.

For the comparison of the optical performance of the MgF_2-based BRs EQEs were measured. Fig. 4 shows the spectra for selected µc-Si:H solar cells, with n-Si as n-type layer, from the set that was completed with MgF_2(80nm)/Ag with the shadow mask approach (blue line) or with ultrathin non-intentionally patterned MgF_2 layer (magenta and dark-cyan lines). The EQEs before and after thermal annealing, when available, are compared to the baseline cell with standard ZnO:Al(80nm)/Ag BR and to the cell with the novel n-SiO_x/Ag BR where the n-SiO_x layer simultaneously plays the role of n-layer in the p-i-n junction and buffer layer between Si and Ag [13,14]. No EQE could be measured after thermal annealing for the cells with 2 and 4 nm thick MgF_2, while an improvement in the EQE was achieved for the cell completed with the MgF_2(80nm)/Ag BR, although the treatment had negative impact on R_s. Nevertheless in this preliminary test none of the BRs with MgF_2 reaches the performance of the standard BR, likely because of collection issues. The non-ideal MgF_2 coverage obtained with the shadow mask also contributes. In addition superior performance is again demonstrated with the n-SiO_x/Ag BR, as in previous reports [13,14].

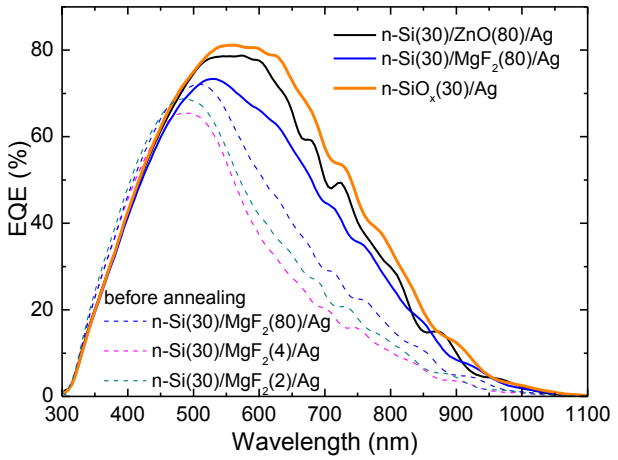

Fig. 4. EQEs of µc-Si:H solar cells completed with 80 nm-thick MgF_2 patterned with shadow mask plus Ag, ultrathin non-intentionally patterned MgF_2 (2 and 4nm) plus Ag, standard ZnO:Al(80nm)/Ag BR, dual function n-SiO_x(30nm)/Ag BR. BR and n-type layer are specified in the legend.

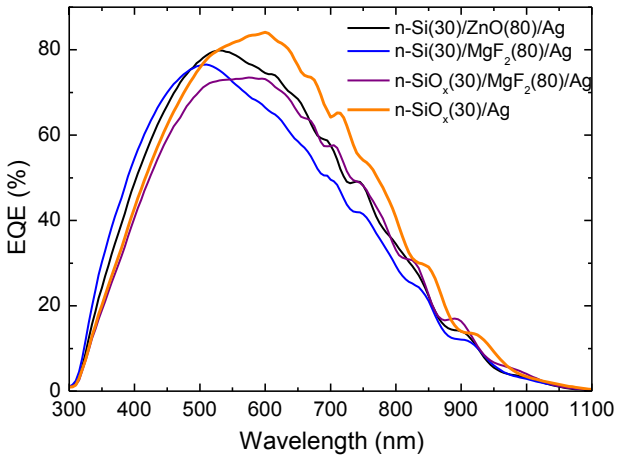

Fig. 5. EQEs of µc-Si:H solar cells with MgF_2 buffer layer in the BR patterned by photolithography compared to cells completed with standard ZnO:Al(80nm)/Ag BR and dual function n-SiO_x/Ag BR. BR and n-type layer (n-Si or n-SiO_x) are specified in the legend.

Fig. 5 shows the EQEs of cells from the set with MgF_2 patterned by photolithography. Examples with MgF_2(80nm)/Ag BR both in the case of n-Si (blue solid line) and n-SiO_x (purple line) n-type layer are included. The EQEs in fig. 4 and 5 cannot be directly combined in a joint comparison because of non-intentional variation of the crystalline phase fraction in the µc-Si:H absorber layer caused by slightly different conditions in the deposition chamber for the two sets of cells. Here the MgF_2-based BR performance is compared again to the standard ZnO:Al(80nm)/Ag BR and to the novel n-SiO_x/Ag BR from the present set of cells. Also in this case the BRs with MgF_2 do not reach the performance of the standard BR, although similar EQE values at large wavelengths as for the reference cell have been measured when using n-SiO_x as n-type layer. Again superior performance has been observed with the n-SiO_x/Ag BR.

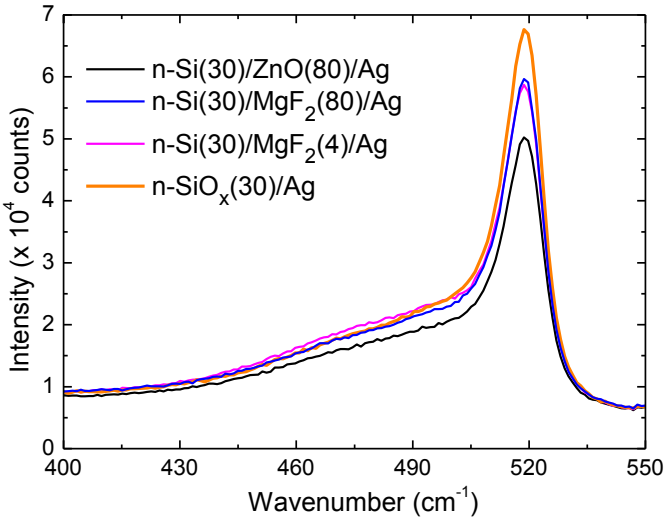

Fig. 6. Raman spectra at excitation wavelength of 785 nm measured on 1µm-thick µc-Si:H solar cells with different BRs (solid lines). BR and n-type layer are specified in the legend.

As electrical issues might have likely masked the optical performance of the MgF_2-based BRs, the full potential has been finally estimated by means of absolute Raman intensity measurements through the entire cell structure with excitation wavelength of 785 nm, where the effect of the BR is relevant. As pointed out in ref. [15], the peculiarity of this technique is to overcome the collection issues that affect the EQE and to look at the contribution of the Si layers only, differently from the reflectance measurements that include parasitic absorption in the contact layers. For measurements with weakly absorbed light, the Raman signal for Si is proportional to the optical thickness of the Si layer, which depends on the BR scattering ability. Also, more Raman photons and then larger Raman intensity is measured if more light is available, as in the case of reduced parasitic absorption losses in the BR. Relative changes of the intensity can be then used to compare BR capabilities at providing improved absorption into Si, as here front TCO and physical i-layer thickness are unchanged. Fig. 6 shows the Raman spectra for relevant solar cells from the set shown in fig. 4, acquired as explained in the Experimental section in order to obtain reliable absolute intensities (solid lines). The lowest intensity of the Si peak is obtained with the conventional ZnO:Al(80nm)/Ag BR (black line). An increase is measured with the MgF_2(80nm)/Ag BR (blue line) and, interestingly, nominal 4nm of MgF_2 (magenta line) provide an equivalent effect as the thicker layer. The Raman investigation confirms then the expected superior performance of MgF_2/Ag BR thanks to low *n* and no free-carrier absorption and establishes in addition the good potential of the ultrathin approach. Nevertheless, both the designs with MgF_2 do not surpass the performance of the dual-function n-SiO_x/Ag BR (orange line in fig. 6), which remains a very efficient BR despite the simplicity of the design.

4. Conclusions

The light-management potential of different Ag-based BR configurations applied to µc-Si:H solar cells has been explored. In particular, evaporated MgF_2 with lower refractive index and no free-carrier absorption has been investigated as a potentially more efficient buffer layer between Si and Ag with respect to standard ZnO:Al. The novel dual-function n-SiO_x/Ag BR has been also included in the comparison. No clear conclusions have been reached from EQE spectra due to collection issues caused by the still non-optimal electrical contacting schemes. However, thanks to complementary Raman intensity measurements at long wavelenghts, where the effect of the BR is relevant, improved absorption of the long wavelength light into Si has been observed with MgF_2/Ag BR versus

the standard BR. In addition the strong potential of ultrathin (few nm) non-continuous MgF_2 layers has been established. Nevertheless, the novel dual-function n-SiO_x/Ag BR outperforms all the BR configurations in this work.

Acknowledgements

This work was carried out in the framework of the FP7 project “Fast Track”, financed by the EC under contract number 283501.

References

[1] Krč J, Lipovšek B, Topič M. Light Management in Thin-Film Solar Cell. In: Cristobal A, Martí Vega A, Luque López A editors. Next generation of photovoltaics. Springer-Verlag Berlin Heidelberg; 2012. p. 95-129.
[2] Sai H, Jia H, Kondo M. Impact of front and rear texture of thin-film microcrystalline silicon solar cells on their light trapping properties. J Appl Phys 2010;108:044505.
[3] Hüpkes J, Owen JI, Bunte E, Zhu H, Pust SE, Worbs J, Jost G. New texture etching of zinc oxide: tunable light trapping for Si thin film solar cells. In: Proc. 25th European Photovoltaic Solar Energy Conference, Valencia, Spain; 2010. p. 3224-3227.
[4] Boccard M, Battaglia C, Hänni S, Söderström K, Escarré J, Nicolay S, Meillaud F, Despeisse M, Ballif C. Multiscale transparent electrode architecture for efficient light management and carrier collection in solar cells. Nano Lett 2012;12:1344-1348.
[5] Battaglia C, Hsu C-M, Söderström K, Escarré J, Haug F-J, Charrière M, Boccard M, Despeisse M, Alexander DTL, Cantoni M, Cui Y, Ballif C. Light trapping in solar cells: can periodic beat random? ACS Nano 2012;6:2790-2797.
[6] Sai H, Saito K, Hozuki N, Kondo M. Relationship between the cell thickness and the optimum period of textured back reflectors in thin-film microcrystalline silicon solar cells. Appl Phys Lett 2013;102:053509.
[7] Paetzold UW, Smeets M, Meier M, Bittkau K, Merdzhanova T, Smirnov V, Michaelis D, Waechter C, Carius R, Rau U. Disorder improves nanophotonic light trapping in thin-film solar cells. Appl Phys Lett 2014;104:131102.
[8] Moulin E, Paetzold UW, Bittkau K, Owen J, Kirchhoff J, Bauer A, Carius R. Investigation of the impact of the rear-dielectric/silver back reflector design on the optical performance of thin-film silicon solar cells by means of detached reflectors. Prog Photovolt: Res Appl 2013;21:1236-1247.
[9] Haug F-J, Söderström T, Cubero O, Terrazzoni-Daudrix V, Ballif C. Plasmonic absorption in textured silver back reflectors of thin film solar cells. J Appl Phys 2008;104:064509.
[10] Lipovšek B, Krč J, Isabella O, Zeman M, Topič M. Modeling and optimization of white paint back reflectors for thin-film silicon solar cells. J Appl Phys 2008;108:103115.
[11] Kang D-W, Sichanugrist P, Konagai M. Novel application of MgF_2 as a back reflector in a-SiO_x:H thin-film solar cells. Appl Phys Express 2014;7:082302.
[12] Holman ZC, Descoeudres A, De Wolf S, Ballif C. Record infrared internal quantum efficiency in silicon heterojunction solar cells with dielectric/metal rear reflectors. IEEE J Photovolt 2013;3:1243-1249.
[13] Delli Veneri P, Mercaldo LV, Usatii I. Silicon oxide based n-doped layer for improved performance of thin film silicon solar cells. Appl Phys Lett 2010;97:023512.
[14] Mercaldo LV, Delli Veneri P, Mercaldo LV, Usatii I, Esposito EM, Nicotra G. Broadband near-field effects for improved thin film Si solar cells on randomly textured substrates. Sol Energy Mater Sol Cells 2013;112:163–167.
[15] Ledinsky M, Moulin E, Bugnon G, Ganzerova K, Vetushka A, Meillaud F, Fejfar A, Ballif C. Light trapping in thin-film solar cells measured by Raman spectroscopy. Appl Phys Lett 2014;105:111106.
[16] Delli Veneri P, Mercaldo LV, Tassini P, Privato C. Correlation between structural properties and performances of microcrystalline silicon solar cells. Thin Solid Films 2005;487:174–178.
[17] Delli Veneri P, Mercaldo LV, Privato C. Deposition pressure effects on material structure and performance of micromorph tandem solar cells. Ren Energy 2008;33:42–47.